

How the movement characteristics of large marine predators affect estimates of their abundance

Fabio Boschetti^{1,2}, Mathew A. Vanderklift¹

¹ CSIRO Oceans & Atmosphere Flagship, Private Bag 5, Wembley, 6913, Australia

² School of Earth and Geographical Sciences, The University of Western Australia
35 Stirling Highway, Crawley 6009, Western Australia

Abstract

Understanding animal movement provides information that helps design effective conservation initiatives. We intuitively understand that the way animals move at large scales determines the extent of their home range and their migratory patterns – and we know that these features are relevant to decisions about the location, size and distribution of protected areas. It is less intuitively obvious that knowledge of movement characteristics at finer scales can also have conservation implications. By modelling the small to intermediate scale movement (1 to 10³ metres) of a large marine predator in a shallow coastal environment, we show how different assumptions about movement patterns influence estimates of species abundance derived from field observations. Foraging behaviour, statistical properties of the swimming path and average speed exert the greatest impact, suggesting that these should be the focus of further experimental work. Better data would inform our understanding and considerably reduce the uncertainty in abundance estimation, improving conservation-related decision making.

Keywords: animal movement; animal abundance; agent based modelling; shark behaviour.

Highlights

- Assumption about fine scales (1-1000 m) movement can have a considerable impact on estimation of animal abundance.
- This also applies to estimates of abundance uncertainty.
- We demonstrate this by modelling shark movement via Levy-flights and correlated random walks
- Foraging behaviour, statistical properties of the swimming path and average speed have the largest impact.
- We demonstrate the approach on real data from remote underwater video surveys of sharks in coastal waters.
-

1 Introduction

Estimates of the abundance of large predators helps inform choices about which species and which areas need protection, and monitor the effectiveness of protection [1, 2]. The abundance of large predators cannot usually be observed directly, but can only be inferred indirectly from counts of individuals, which is usually obtained from very sparse spatial and temporal sampling. Estimating abundance from individual counts is further complicated because predators move and it can be difficult to discriminate between different individuals. It follows that the way predators move affects i) the probability of detecting an individual at a given location during a certain time interval and ii) the probability that two separate detections are due to two different individuals, rather than a single individual seen twice.

Detailed understanding about how marine predators move is still lacking so we need to make some assumptions. Often, this is done without making the assumptions explicit. The aim of this paper is to show how these assumptions affect estimates of marine predator abundance obtained from camera surveys, using remote underwater video surveys of sharks (e.g. [3]) as a test system. Identifying which assumptions have the greatest influence on estimates of abundance provides information about which components of a predator's movement deserve more experimental attention, and the extent to which this will help conservation decisions.

Computer models of animal behaviour have been used to simulate field surveys in order to assess species abundance and distribution or to test survey design [3-11]. Depending on model complexity, these approaches

require the model *developer* to make explicit (in the computer code) a number of assumptions about movement patterns. Very simple models may approximate animal movement by Brownian motion leading to diffusion-like area cover [12]. A model *user* may then need to provide the size and centres of home ranges. As an output, the model may provide, say, the probability of detecting an animal at different positions in space. This, obviously, depends on the assumed movement type (in this case Brownian motion). However, *how* detection probability depends on the assumed movement type may or may not be clear to the model user. At the other extreme, more complex models may allow the user to control a larger number of movement parameters, including the animal's speed, the type of movement (e.g. Brownian vs Correlated Random Walk), preferential directionality, time dependence, space dependence, and so on. The requirement to provide many parameters entails more a-priori biological knowledge, which is often lacking. Some users may feel that in these circumstances, uncertainty in model outcomes increases with model complexity. However, these requirements highlight that if movement assumptions are not made explicitly by the model user, they are made implicitly by the model design, often leaving the user unaware of both these choices and their implications. Only once these assumptions are made explicit will the user be able to appreciate the potential impact these choices can have on the model's behaviour.

In this work we provide an example of how uncertainty in some parameters controlling animal movement can affect estimates of species abundance. We describe a model to simulate the movement of blacktip reef sharks (*Carcharhinus melanopterus*) in coastal reefs. We then use this model in an inverse mode [13, 14] to estimate shark abundance. By showing which movement parameters most affect abundance estimation and uncertainty, we also provide information on which of these parameters further experimental work should focus.

We describe all equations used in the model and provide the information needed to reproduce our results. We emphasise visual description of our results with the specific aim of the development of an intuition for how features of a species' movement patterns influence estimates of abundance. We start by reviewing some approaches commonly used to model animal movement. We then treat the estimation of predator abundance as an inverse problem and show how a model of animal movement can be used to fit observations from underwater video cameras. We proceed by describing the model used in this work and show how parameters controlling the modelled predator movement impact visitation patterns and, in turn, abundance estimation. In doing so, we model realistic settings in shallow reef environments from Western Australia and apply our results to a real data set. We conclude by discussing the implications of our results in terms of future experimental work and its potential impact on decision-making in marine conservation.

2 Analysis of animal movement

Animal movement can be analysed at a number of levels, each characterised by its own implicit temporal and spatial scale [15-20]. Here we consider four levels of analysis. At the finest level, we have what [15] define as 'fundamental movement elements', which animals perform in their daily activities (e.g. stepping, speeding, lounging, stopping, standing) and which are mostly determined by the physical and physiological characteristics of the species. At the next level, fundamental movement elements are combined to carry out specific activities (e.g. habitat choice, foraging, avoiding predation, mating, resting). These represent 'decisions' and reactions carried out at scales of fractions of seconds to minutes and can be seen as incorporating the 'causal' mechanics responsible for animal movement. At the third level, longer time series of unit movements result in geometric patterns at the scale of minutes to days and meters to kilometres, depending on the species. These geometric patterns are usually analysed in terms of shape, spatial extent covered and search and foraging efficiency, which can be interpreted as global properties emerging from actions at finer scales. While the first level describes the mechanics and the second level supposedly includes the immediate 'causes' of movement, the third level can be seen as providing an additional evolutionary feedback resulting from its adaptive efficiency [21-31]. In the literature the first and second levels of analysis are usually referred to as 'mechanistic', while the third level is often referred to as 'statistical' [32, 33]¹.

The fourth level is represented by the actual field observations. Data collection is usually carried out at a scale intermediate between the mechanistic and statistical levels, but at a resolution considerably sparser than both. This is where much of the debate on whether the statistical movement patterns of large predators are best described by Lévy flights, Brownian Motion or Correlated Random Walks arises [34-37]. In most circumstances, including the

¹ This terminology may lead to the misleading conclusion that the 'mechanistic' processes are deterministic and algorithmic and that stochasticity belongs only to the statistical framework. Nevertheless, here we decided to adopt this terminology out of consistency with current literature.

datasets we have collected, discriminating between these statistical distributions is difficult [24, 32, 38, 39] because they are affected by how the animal movement depends on the local environment and the distribution of prey, as well as by distortions imposed by the resolution or rate of measurements [11, 40-44]. As a result, it is important to think of field observations as a product of the complex interactions between an animal's actions and the features which constrain (e.g. physical obstacles) or alter (e.g. prey-predator distribution, habitat distribution, currents, winds) these actions [15].

Information about movement of large marine predators is mostly derived from studies of oceanic species, undertaken in the open ocean, which can be considered essentially unbounded [45]. In coastal reef ecosystems this is rarely, if ever, the case. When information does come from coastal ecosystems, the constraints imposed on animal movement by physical obstacles are rarely explicitly discussed. Even if we had high resolution observations and their impact was discussed, unravelling the unconstrained movement patterns from the effect of the constraints would be very difficult. As a result care should be used in adopting statistical movement characteristics observed in one environment (open ocean, say) to a very different one (coastal ecosystems).

3 Estimating population abundance from field observations

In a previous study [3], we cast the assessment of shark abundance as an inverse problem. Observations of individual animals do not provide direct estimates of abundance. However, given a suitable model of the individual's behaviour, the model can be fitted to the observations, thus indirectly providing an estimate of abundance, among other parameters, and the associated uncertainty. Several algorithms could be used to carry out the inversion numerically [13, 14, 46]. The results from the inversion could also be visualised to help the user gain insights into model parameter uncertainty and carry out an approximate sensitivity analysis [47-49]. Alternatively, parameter uncertainty and a priori ecological knowledge could be formally included in the analysis via Bayesian approaches [50, 51], including Bayesian Hierarchical Modelling [52-56]. An application to a similar problem can be found in [57]. Some of these approaches can be computationally very expensive, in particular when a large set of model parameters needs to be inverted. In this work we extend the approach used in [3] by using a combination of visual and fairly simple statistical analysis to determine which feature of an individual's movement most influences the estimates of density.

Figure 1 summarises the approach (see [3] for more details). Figure 1a shows a shallow water environment, where black is the land (coast and reef crests) and blue and white water (white corresponds to an assumed foraging habitat which will be introduced below). This spatial domain represents a realistic habitat for blacktip reef sharks, and is based on a location within the Ningaloo Marine Park in Western Australia (within the Mandu Sanctuary Zone, approx coordinates 113.52E, 22.05S), where this species is abundant [3] (see Figure 16 below). The red marks show the position of underwater video cameras which record for 1 to 3 hours. The camera view is determined by the camera orientation, the aperture angle (which we measured at 45 degrees) and the maximum distance from the camera at which predators can be discriminated (discussed below). In dark blue we see the simulated paths of 2 individual sharks, as obtained via the movement algorithm we describe below. For each shark s ($s=1 \dots S$) and each camera c ($c=1 \dots C$) we calculate the time $t_{s,c}$ the shark s would theoretically be visible on camera c and we define

$$F_{mod} = \frac{\sum_{s,c} t_{s,c}}{T C}, \quad (1)$$

where T is the duration of the simulation, C the number of cameras and the subscript *mod* indicates 'modelled' results. F_{mod} thus estimates the average length of time we expect to see a shark in the video recording. Similarly, we analyse the actual underwater video camera footage and we calculate the time the actual sharks are visible, from which we obtain an analogue measure F_{obs} (where *obs* indicates 'observations').

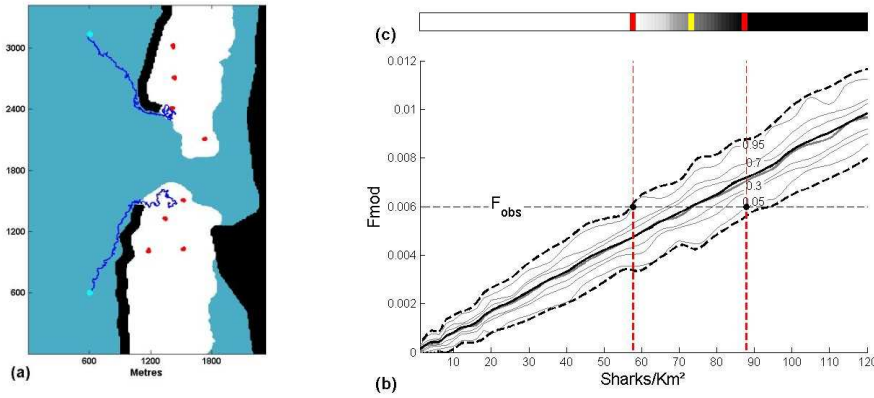


Figure 1. (a) The test area used in the simulations discussed in the study. It corresponds to a location within the Mandu Sanctuary Zone within the Ningaloo Marine Park in Western Australia, The red pixels show the area covered by the camera's view. The blue lines show the swimming paths of two sharks, starting from the cyan dots. (b) F_{mod} plot. For a given shark density (X axis) we plot different values of F_{mod} (Y axis) resulting from multiple simulations of different parameter combinations. The horizontal dashed line indicates F_{obs} obtained from observations. This line intersects the 5th and 95th percentiles of the F_{mod} distribution for shark densities of 58 and 88 sharks/km² respectively. (c) Cumulative probability distribution over different shark densities for the specific F_{obs} obtained from observations. The yellow and red bars show the 50, 5 and 95 percentiles, respectively.

F_{mod} is a function of the density of individual sharks as well as of a number of parameters controlling each sharks' behaviour (see model description below). We can obtain an estimate of the distribution of F_{mod} via a Monte Carlo approach, by running our model for different parameter combinations. To account for the inherent stochasticity in the simulations, we can carry out multiple runs for each parameter combination. An example of this distribution is shown in Figure 1b, where for each shark density on the X axis, we plot the corresponding distribution of F_{mod} resulting from the simulations.

The last step in our approach involves determining which densities correspond to values of $F_{mod} \approx F_{obs}$. As an example, in Figure 1b, the horizontal line $F_{obs} = 6e^{-3}$ intersects the 5th and 95th percentiles of the F_{mod} distribution corresponding to densities of 58 and 88 sharks/km² respectively. This gives us an indication of the likely shark density in the area as well as an approximate estimation of its uncertainty. The cumulative probability distribution over the shark densities for $F_{obs} = 6e^{-3}$ is also shown in Figure 1c, where the yellow and red bars show the 50, 5 and 95 percentiles, respectively. In the rest of the document we refer to this as a F_{mod} plot. For sake of simplicity, we temporarily assume F_{obs} is a precise measurement with zero error, a requirement we will relax later on.

4 A model of movements by large marine predators

In this section we describe a model of movements by large marine predators (that could also be extended to other fauna). It consists of four modules: i) unoriented stochastic movement, ii) oriented stochastic movement, iii) obstacle avoidance and iv) interaction with other individuals of the same species.

The unoriented stochastic movement module generates a random walk and aims to simulate the paths followed within a constrained area, usually represented by a specific habitat. The level of correlation in the random walk, together with other statistical properties of the resulting path, is controlled by a number of adjustable parameters and is described in Section 4.1. In this module, memory is represented in a fairly abstract sense by the time lag within which the animal movements are correlated.

The oriented stochastic movement module generates an oriented path between two locations and aims to simulate a 'purposeful' movement towards a specific area. Here memory is modelled explicitly as the animal's ability to remember how to reach the target location.

The obstacle avoidance module is used to steer clear of fixed obstacles like the coastline and exposed reefs. Finally, repulsion or attraction towards other individuals implements a simple form of interaction with other members of the same species.

4.1 Unoriented stochastic movement

The path generated by an animal movement can be thought of as a series of individual steps, each step consisting of a straight segment, where the angles between two straight segments are defined as turning angles. Different distributions of step lengths and turning angles can result in very different movement paths. Most animal movement models described in the literature can be broadly divided into 2 classes, depending on whether the main focus is on the distribution of step lengths or turning angles. Models belonging to the first class usually choose the step lengths according to a specific statistical distribution and assume random, uncorrelated turning angles. Lévy flights are a common example of this class of models, in which the step distribution is self-similar over a number of spatial scales [39, 58-60]. Models belonging to the second group choose the turning angles according to a specific distribution and employ constant or random uncorrelated step lengths. Brownian motion and various forms of correlated random walk belong to this class of models.

Viewing these two classes as arising from two different generating processes is both intuitively and mathematically meaningful since the resulting movement patterns are not equivalent. For example, in the first class smoothly-curved paths are extremely unlikely to arise since the turning angles are uncorrelated, while in the second class they can be generated by a suitable distribution of turning angles, as we will see below. Similarly, in the case of Lévy flights, extremely long steps are rare but likely to occur, but are unlikely to occur in the second approach given that they would require extremely long series of zero turning angles.

To implement correlated random walks we follow the approach described in [30]. The turning angles are chosen from the following circular distribution [61]:

$$P_{\gamma,\kappa}(\theta) = \frac{(\cosh(\gamma\kappa) + \sinh(\gamma\kappa) \cos(\theta))^{1/\gamma}}{2\pi P_{1/\gamma}(\cosh(\gamma\kappa))}$$

Equation 2

where, θ is the turning angle and $P_{1/\gamma}$ is the associated Legendre function of the first kind of order 0 and degree $1/\gamma$. For a given turning angle θ , Equation 2 gives the probability of the predator making a change in swimming direction of angle θ . This probability distribution depends on two parameters $-\infty < \gamma < \infty$ and $\kappa \geq 0$. By varying these two parameters, Equation 2 generalises most of the standard symmetric circular distributions [61, 62] including some employed to model certain types of animal movement [63]. For $\kappa=0$, Equation 2 generates the uniform circular distribution, which leads to Brownian motion.

[25] show a number of different movement paths as a function of different γ and κ combinations in Equation 2, as well as some properties of the resulting paths, including the mean cosine angle $\rho = \langle \cos(\theta) \rangle$ and the correlation length $\tau = -1/\ln(\rho)$. The mean cosine angle gives an indication of the directional persistence of a path (the closer to 1, the more linear the path is) while the correlation length, which represents the amount of correlations in successive steps along the path, gives an indication of the directional memory. For a more general analysis of the types of behaviours arising from Equation 2 we refer the reader to [61]. In this work, we chose six combinations of γ and κ leading to different values of ρ and τ and thus to six qualitatively different movement paths, which we refer to as JP1-JP6 in the rest of the document (JP indicates the initial of the authors in [61]). As discussed above, Brownian motion (BM) is obtained by modelling a JP distribution with $\kappa=0$.

As modelled in [7], the self-similar distribution of step lengths for the Lévy walks follows

$$P(r) \sim r^{-\mu} \text{ for } r \in [l_{min}, l_{max}]$$

Equation 3

where $P(r)$ is the probability of occurrence of a step of length r , l_{min} and l_{max} are the minimum and maximum step lengths, respectively ([45, 64]) and μ is the scaling exponent, which determines how step lengths are distributed within this range. Following [7], we chose three Lévy walk exponents $\mu = [1.7, 2, 2.3]$, to represent three alternative forms of Lévy walk. Empirical observations suggest that Lévy flights resulting from these exponents are suitable for modelling foraging animal behaviour ([65-68]), including sharks ([45, 64, 69]). These values are distributed around $\mu=2$, which some studies suggest provides an optimal search pattern ([45, 64, 69-72]). In the rest of the document we refer to these Lévy walks as LW1-LW3.

When it comes to numerical implementation, JP and LW paths can be generated by very similar algorithms. Given a specified l_{min} in Equation 3, a step in a Lévy flight can be equivalently seen as i) a single step $n \times l_{min}$ length between two changes of direction or ii) n steps of length l_{min} without a change of direction. The latter is equivalent to a sequence of $n-1$ 0° turning angles. This also provides a simple way to compute the mean cosine angle for Lévy flights.

This overall approach provides 10 alternative path types (JP1-JP6, BM, LW1-LW3). Because we lack detailed empirical information about which of these best describes the movement of *C. melanopterus*, we employ all 10 alternative path types to reflect uncertainty in sharks' movement behaviour and study their impact on the estimation of shark abundance. Table 1 summarises the parameters and resulting statistics for each path type, and Figure 2 shows the angle distribution for JP1-JP6.

Table 1. Parameters and mean cosine angle of swimming paths resulting from the 10 path types.

Modes	Equation	Parameters	Mean cosine angle
JP1	Equation 2	$\gamma = -.1; \kappa = 5.01$	$\rho = .93$
JP2	Equation 2	$\gamma = -1; \kappa = 1.86$	$\rho = .73$
JP3	Equation 2	$\gamma = 0.03; \kappa = 6$	$\rho = .9$
JP4	Equation 2	$\gamma = -2; \kappa = 1$	$\rho = .43$
JP5	Equation 2	$\gamma = 1; \kappa = 3.8$	$\rho = .5$
JP6	Equation 2	$\gamma = 1.95; \kappa = .93$	$\rho = .29$
BM	Equation 2	$\kappa = 0$	$\rho = 0$
LW1	Equation 3	$\mu = 1.7$	$\rho = .82$
LW2	Equation 3	$\mu = 2$	$\rho = .73$
LW3	Equation 3	$\mu = 2.3$	$\rho = .62$

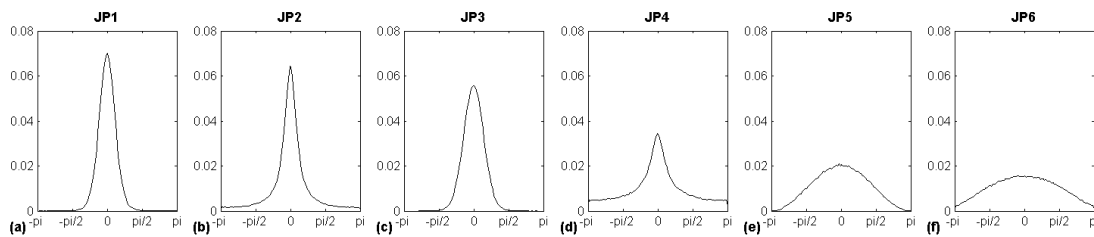


Figure 2. Circular distributions of turning angles for path types JP1-JP6, showing the probability of occurrence (Y axis) of a given turning angle (X axis).

Figure 3 shows an example of the path of an individual shark for each path type, where the plots are shown at different resolution in order to allow the visual inspection of the path's small scale details. Figure 4 shows the paths of 10 sharks, each starting from the same position; here the paths are plotted at the same scale, to illustrate the spatial extent of paths encompassed by individuals following different path types.

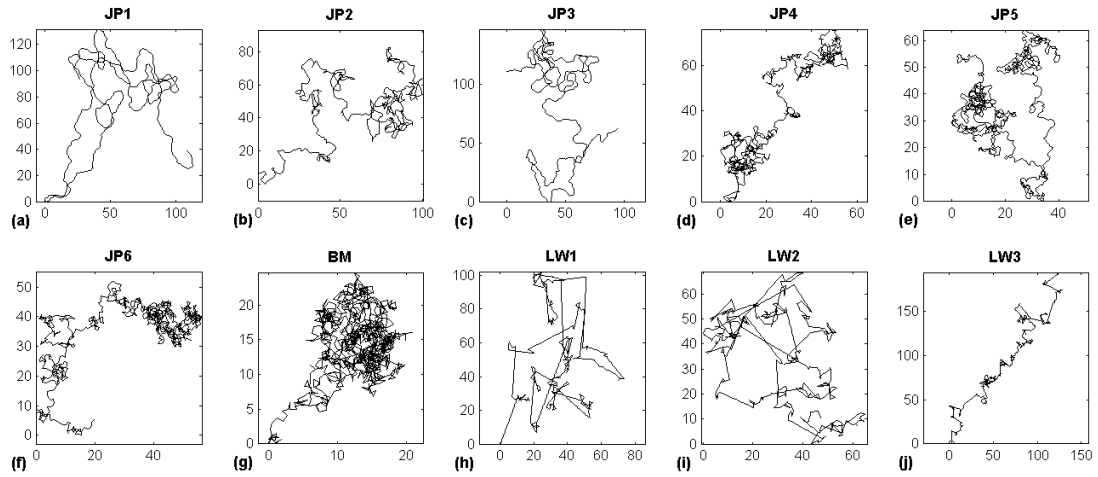


Figure 3. Path of a single shark (1000 time steps) swimming in an obstacle-free area for the different path types. Plots are shown at different resolution to highlight the path's small scale details.

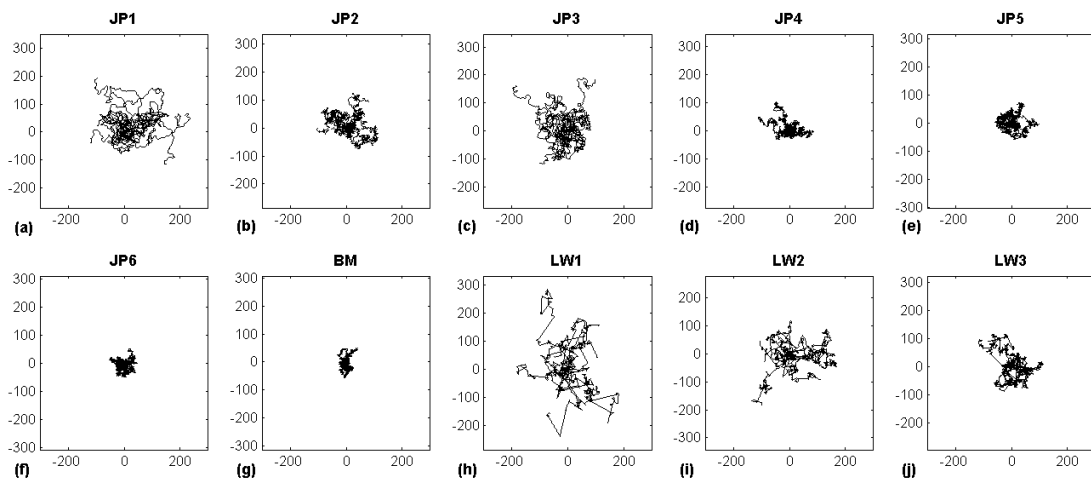


Figure 4. Paths of 10 sharks (1000 time steps), each starting at position (0,0). Plots are shown at the same resolution to highlight the area cover resulting from different path types.

Figure 5 shows the pattern of site visitation generated by modelling 9 sharks (equivalent to a density of ~ 40 sharks/ km^2) swimming for 6 hours, in an obstacle-free area (the blue background indicates water). Locations visited by a shark are coloured according to the number of times the pixel has been visited (red to yellow tones map lower to higher visitation rates; blue means no visitation). A simple visual inspection shows how visitation patterns differ between some path types. Brownian Motion (Figure 5g) provides the most clustered visitation pattern, which results in larger areas of low or no visitation. Among the correlated random walks (JP1-6) JP1 and JP3 result in the most homogenous visitation pattern, and JP6 is the one closest to Brownian Motion (BM). Among the Lévy walks, the visitation patterns become less homogenous with increasing exponent μ (LW1 to LW3). By comparing this with Figure 4, we see that these visitation patterns are related to the spatial extent of the shark movement as, a function of the mean cosine angle ρ .

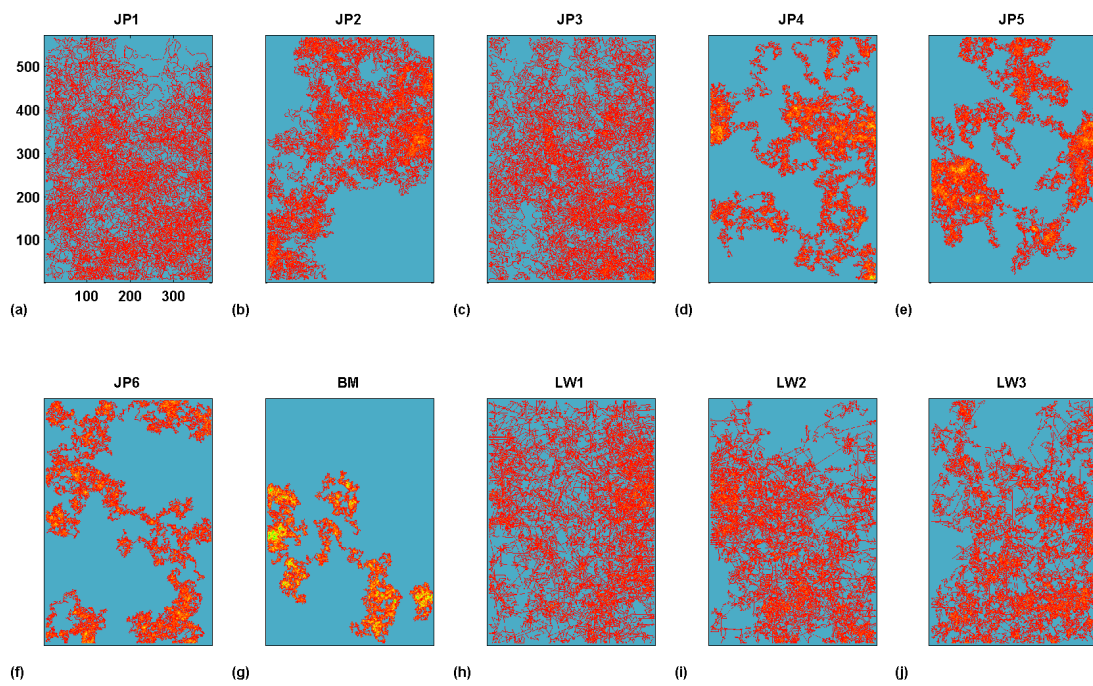


Figure 5. Site visitation distribution for 9 sharks swimming (equivalent to a density of 40 sharks/km²) for 6 hours. The blue background represents an obstacle-free area. A pixel's tone (red to yellow) maps the number of times the location has been visited by a shark, with hotter tones reflecting higher visitation rates (blue maps no visitation).

Figure 6 shows 160 sharks (equivalent to a density of ~20 sharks/km²) for the test area in Figure 1a, which includes reef crests and coastline. The visitation patterns found in Figure 5 can also be recognised in Figure 6, with JP1, JP3 and LW1 giving the most homogenous visitation pattern and JP6 and BM the most clustered.

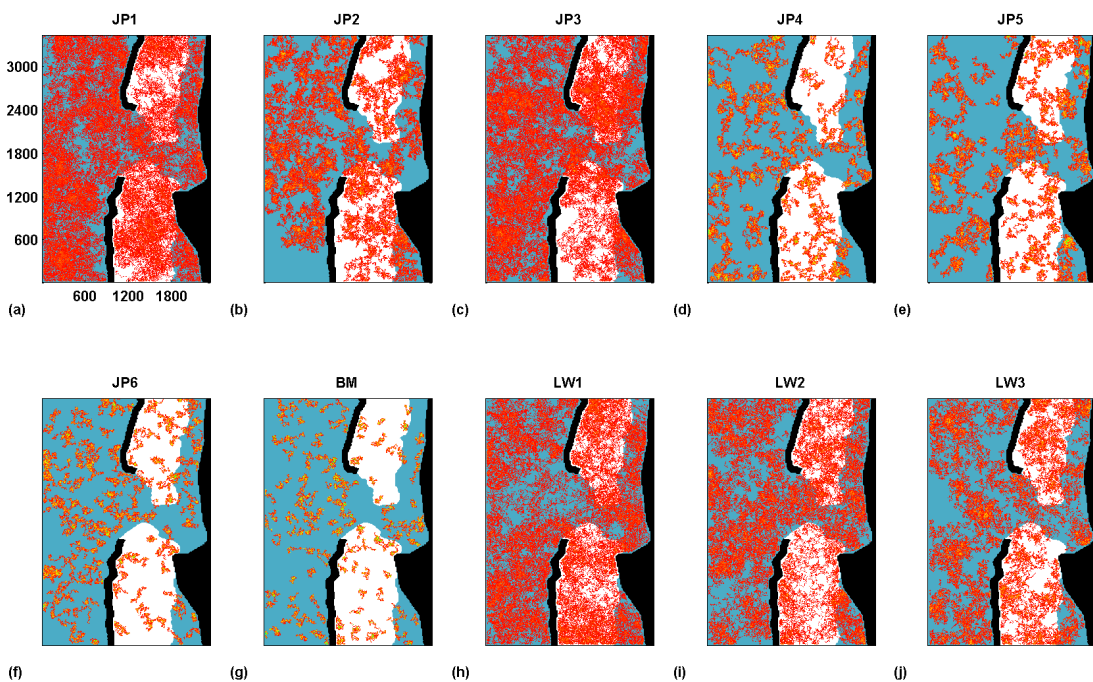


Figure 6. Site visitation distribution for 160 sharks (~20 sharks/km²) swimming for 6 hours, in the study area.

For each of the 10 different path types, Figure 7 shows the F_{mod} plots arising from 20 virtual cameras located in the same test area. Given a fictitious F_{obs} value ($2e-3$ in this example) it shows how estimates of shark density, as well as the associated uncertainty, can vary considerably as a function of the movement mode. The uncertainty in the estimates varies dramatically from JP1 ($\sim 28-48$ sharks/km²) at the lower end to BM where the uncertainty is largest ($\sim 33-116$ sharks/km²).

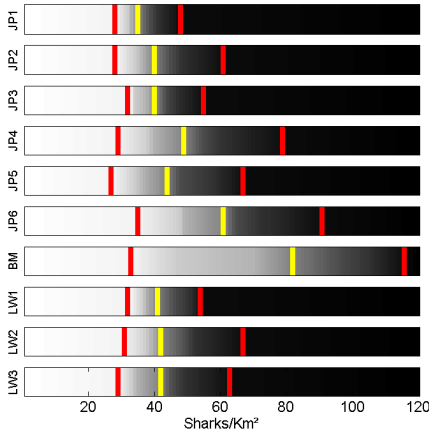


Figure 7. F_{mod} plots for different path types. A fictitious observed value of $F_{obs} \approx 2e-3$ would result in different shark density estimates (yellow vertical bar) and uncertainty (red vertical bars) depending on the assumed path type.

So far we have performed a visual analysis of the swimming paths, visitation rates and estimated shark density along with associated uncertainty. The visual analysis suggests that the path types have a considerable impact on these variables. A simple statistical analysis of the simulation results supports this initial conclusion. For each combination of two path types, we carry out a pair-wise Kolmogorov–Smirnov test (KS test [73]) between the 2 sets of F_{mod} values. The results are seen in Table 2, where bold values show statistical significance ($p < 0.05$). It shows that, for this specific experimental setting, the three Lévy walks cannot be differentiated from one another, JP2 cannot be differentiated from JP3, JP4 from JP5 and finally JP2 and JP3 cannot be differentiated from any of the LW path types.

Table 2. p values from Kolmogorov–Smirnov test between the F_{mod} generated by the different path types .

	JP2	JP3	JP4	JP5	JP6	BM	LW1	LW2	LW3
JP1	2.8e-03	1.5e-05	6.4e-11	3.6e-10	7.5e-20	2.9e-54	2.0e-07	1.1e-06	6.4e-05
JP2		6.8e-01	8.6e-04	4.7e-03	3.8e-09	3.4e-41	1.6e-01	2.0e-01	8.8e-01
JP3			1.1e-02	7.6e-02	2.7e-07	2.2e-39	6.0e-01	9.1e-01	9.4e-01
JP4				6.8e-01	3.3e-02	8.2e-24	1.1e-01	2.1e-02	1.3e-03
JP5					1.3e-03	3.5e-30	9.8e-02	2.5e-01	2.5e-02
JP6						1.7e-15	7.1e-06	1.1e-06	1.8e-08
BM							2.6e-32	6.1e-34	1.3e-37
LW1								9.7e-01	4.4e-01
LW2									6.0e-01

Different experimental settings, including different numbers of cameras, varying camera locations and different geographical features, will have an impact on the ability to discriminate between some path types. We will return to this issue in the Discussion.

4.2 Obstacle avoidance

A shark’s path in shallow water is necessarily constrained by the coastline and reef crests. We model obstacle avoidance as gravitational repulsion (the opposite of gravitational attraction). This is carried out by assigning a gravity value to the land pixels in Figure 1a and generating the corresponding gravity field over the entire spatial domain [74, 75] (see Appendix 3 for implementation details). Figure 8a shows this gravity field. Close to the coastline or a reef crest, the swimming direction θ_u resulting from the unoriented swimming module described above, interacts with the gravity field resulting in a new swimming direction θ' away or parallel to the obstacle.

Figure 1a shows how the gravity field generated by the reef crests allows the two individuals to swim around these obstacles in their path to the foraging area (white area).

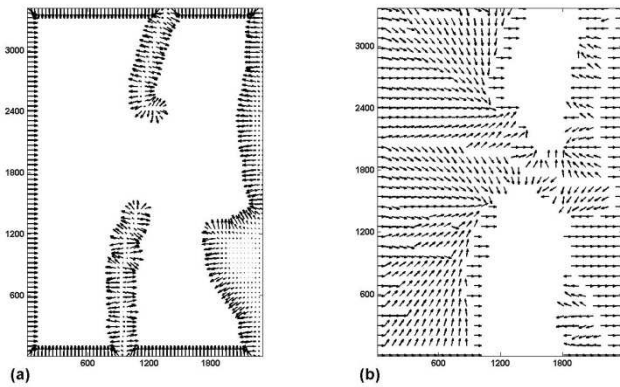


Figure 8. (a) Gravity gradients generated by coastlines and reef, as described in Section 4.2. These repel the sharks and ensure obstacle avoidance. Notice that the domain border is treated as a coastline to prevent sharks from entering or leaving the model domain. (b) For each map location, direction towards the foraging area, (white region in Figure 1a) as described in Section 4.3. This is pre-calculated to speed up the computational effort during a simulation.

4.3 Oriented stochastic movement

Some species of large predators visit specific areas at certain times of the day, often to forage. In this work, we model this movement component via an additional field which is superimposed to the spatial domain. In Figure 1a the white area represents reef flat habitat, assumed to be a desired foraging habitat for *C. melanopterus*. A parameter k_{dir} is used to orient an individual's movement towards this area as

$$\theta' = (1 - k_{dir})\theta + k_{dir}\beta, \quad k_{dir} \in [0,1]$$

where β is the direction towards the reef flat. For $k_{dir}=0$ the movement is unoriented and an individual follows a path along a direction θ , as described above, while for $k_{dir}>0$, the movement is adjusted towards the reef flat. $0.05 < k_{dir} < 0.3$ has been suggested to provide a realistic description of animal movement [76] and the values $k_{dir}=[0, 0.05, 0.1]$ are used in this work.

The parameter k_{dir} can be used to model a species' behaviour at different times of the day, under the hypothesis that some species of sharks do not tend to forage at noon ($k_{dir}=0$), and they are more active at dusk [3] ($k_{dir}>0$). Here, choosing the two values $k_{dir}=[0.05, 0.1]$ allows us to represent the uncertainty in how individuals move towards the target area.

As an example, Figure 1a shows the path of two individual sharks following a JP3 path type, with $k_{dir}=0.1$. The sharks start swimming outside the reef (cyan dots) and swim towards the reef flat (white) avoiding the reef crest. At each step, the direction chosen by each shark is a weighted sum of the stochastic value drawn from the JP3 turning angle distribution, the repulsion from the coastline and the attraction towards the reef flat.

For each location in the model domain, the direction to an area (β) is calculated with the algorithm described in Appendix 2. This algorithm can be computationally expensive. However, since β is not affected by an individual's movement (and thus does not change in time), it is possible to pre-calculate a field $B = \beta(x,y)$ for each map position (x,y) and store it for later use. This leads to a considerable increase in the speed of simulations. Figure 8b shows the field $B = \beta(x,y)$ for the spatial domain in Figure 1a.

Figure 9 shows the visitation rates for 160 sharks (equivalent to a density of ~ 20 sharks/km²), as in Figure 6, with $k_{dir}=0.1$. Following the KS test results in Table 2, in Figure 9 we show the visitation patterns for only 5 path types. The impact of the spatial constraints on the sharks' paths now becomes evident. Because the sharks need to swim around the reef crest to reach the reef flat, visitation rates are higher close to the reef edges. The difference in visitation rates between these locations and the rest of the domain is particularly evident for path types JP1 and LW2.

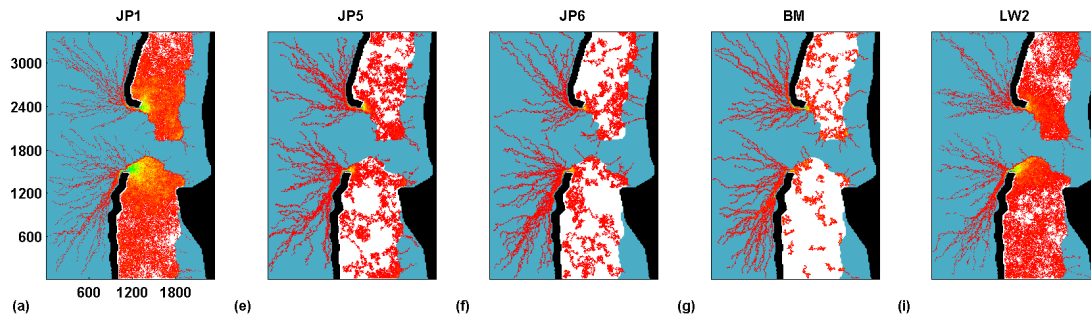


Figure 9. Site visitation distribution for 160 sharks (~ 20 sharks/km²) swimming for 6 hours in the study area with $k_{dir}=0.1$.

5 Interaction with other sharks and video cameras

We know very little about how and at what frequency blacktip reef sharks interact with one another. We have modelled interactions between individual sharks in a similar fashion as obstacle avoidance. Sharks are assigned a fictitious mass value which generates a fictitious gravitational field. When two or more sharks happen to swim within each other's gravitational field, they are influenced by this gravitational field and their swimming path is altered. Details about the implementation are provided in Appendix 3. By choosing the sign, magnitude and spatial extension of the gravitational field, sharks can be repelled or attracted to one another and may interact at different distances. Obviously, a 0 gravity value implies that sharks do not interact.

Figure 10a shows the influence of the gravity field in the case of sharks repelling each other, for the JP1 path type. Here we used a fairly strong gravity field and a large field of influence (20 metres) to emphasise the effect. Obviously, the impact of shark interaction is stronger where the shark density is high and is particularly noticeable where the individuals swim around the reef as shown in the zoomed in panel in Figure 10b. The lack of information about interactions among sharks in nature prevents us from assessing whether the patterns shown in Figure 10 are realistic.

Like interaction between individuals, we know very little about possible interactions between sharks and the systems that we use to observe them – whether these be divers, unbaited or baited cameras. We use unbaited underwater cameras and the visual analysis of the video recordings does not indicate any clear tendency for sharks to be attracted or repelled by the cameras. Attraction or repulsion, should they occur, can however also be modelled by assigning a gravity field to the cameras and by adjusting the field to model shark-camera interactions over different distances.

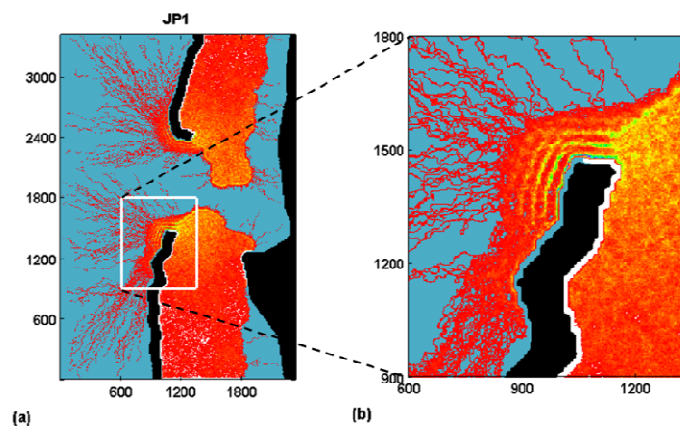


Figure 10. (a) Site visitation distribution for 160 sharks (equivalent to a density of ~ 20 sharks/km²) swimming for 6 hours with $k_{dir}=0.1$ and JP1. (b) Zoomed in region close to the lower reef, where local shark density increases due to the sharks swimming around the reef to reach the foraging area. Here the interaction between the sharks is higher and it impacts the sharks swimming paths.

6 Impact of swimming types on estimates of density

In Section 4.1 we showed how different path types affect estimates of shark abundance. In this section, we use the same approach to analyse the impact of other movement parameters.

In our model sharks move at a constant speed, although the algorithm could be easily modified to include variable speeds. As for other parameters, we have only sparse information on the swimming speed (or distribution of speeds) of sharks in shallow coastal environments. In this section, we represent this uncertainty by using 3 speeds (0.5, 0.7, and 1 m/s) based on literature on *C. melanopterus* and other species of carcharhinid sharks ([77-79]).

Figure 11 shows the F_{mod} plots for the 3 different speeds for JP1. Density estimates and their uncertainty decrease with increasing swimming speed. In other words, misjudging the sharks average speed can result in over-estimating (if the sharks are faster) or underestimating (if the sharks are slower) their abundance. There are two interacting reasons for this result. First, the faster the shark, the larger the area covered during the simulation time, thus the more likely it will cross a camera view. Second, the faster the shark, the quicker it will cross the camera view. Pair-wise KS tests between the sets of F_{mod} values result in the difference between these swimming speeds being all statistically significant ($p < 0.05$, numerical results not shown).

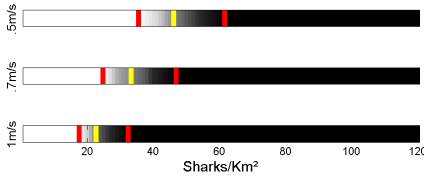


Figure 11. F_{mod} plots for different swimming speeds. The fictitious observed value of $F_{obs} \approx 0.002$ would result in shark density estimates ranging from 37-62 sharks/km² at lower speed to 18-36 sharks/km² at faster speeds.

Figure 12 shows the F_{mod} plots for the 3 different unit step length l_{min} (1, 2 and 3 m). Recall that the role of l_{min} changes according to the path type. For correlated random walks (JP1-6) and Brownian motion, l_{min} is the length of a step between two turning angles. It thus acts as a scaling factor in these swimming modes. In the Lévy walks, l_{min} is the minimum step length (and the most likely step length in the Lévy distribution in Equation 3), but the distribution is scale free between the minimum and maximum step lengths. Notice that l_{min} controls only the step length of unoriented stochastic movement (Section 4.1). For directed movement (Section 4.3), obstacle avoidance and interactions among individuals (Section 4.2), the resolution is determined by the model domain grid spacing (see Appendices 2 and 3). As a result the effective length of a step taken by a shark can be shorter than l_{min} if its path is altered by oriented movement, obstacle avoidance or interaction with other individuals. In other words, l_{min} scales only the unoriented stochastic movement of a shark.

Figure 12 shows that density estimates increase with increasing step length, but that the influence of step length is smaller than the influence of speed and path type. Furthermore, the uncertainty remains approximately constant with varying step lengths. According to the pair-wise KS tests the difference between these step lengths are all statistically significant ($p < 0.05$, numerical results not shown).

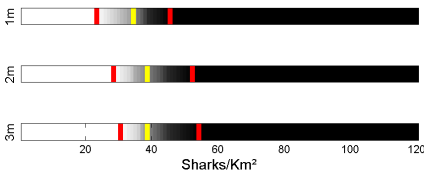


Figure 12. F_{mod} plots for different steps lengths. The fictitious observed value of $F_{obs} \approx 0.002$ would result in shark density estimates slightly increasing from 23-45 sharks/km² to 30-54 sharks/km² with increasing step length, while the uncertainty varies comparatively less.

Figure 13 shows changes in density estimates for an increasing radius determining the extent of interactions between sharks. There is no statistically significant difference between estimates from no interaction (Figure 13 top) and shark repulsion within a 10m radius (Figure 13 middle), while these estimates increase slightly for shark

repulsion within a 20m radius (Figure 13 bottom). Since it is unlikely that sharks may interact with a 20m radius, we tentatively conclude that shark interaction may have an insignificant impact on shark density assessment.

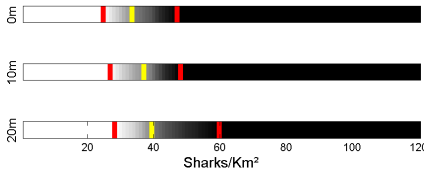


Figure 13. F_{mod} plots for different levels of shark interaction. The fictitious observed value of $F_{obs} \approx 0.002$ would result in shark density estimates of 25-47 sharks/km² for no interaction (top), 27-49 sharks/km² for sharks interacting within a 10m radius (middle) and 28-60 sharks/km² for sharks interacting within a 20m radius (bottom).

Finally, Figure 14 shows the impact of k_{dir} , that is of whether and how individuals are attracted towards the reef flat. The difference between $k_{dir} = 0.1$ and $k_{dir} = 0$ is so large that the uncertainty ranges between the two do not overlap. The difference between $k_{dir} = 0.05$ and $k_{dir} = 0.1$ is much smaller, but still statistically significant ($p = 5e-05$). In [3], different values of k_{dir} were used to model the paths followed by individuals at noon ($k_{dir} = 0$) or dusk ($k_{dir} > 0$), a decision that received some support from patterns obtained from acoustically-tagged individuals. Figure 14 shows how the accurate determination of this parameter can have the largest impact on shark density estimations.

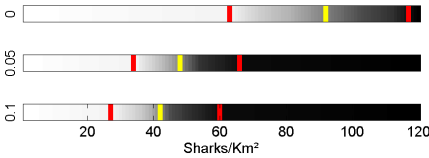


Figure 14. F_{mod} plots for different values of k_{dir} . Shark density estimations vary dramatically from $k_{dir} = 0$ (no attraction toward the foraging area) to $k_{dir} > 0$. Estimates range from 63-117 sharks/km² for from $k_{dir} = 0$ to 27-60 sharks/km² for $k_{dir} = 0.1$ (bottom).

7 A field example

In this section we employ the visualisation tools we described above to assess the uncertainty in shark abundance estimation arising from a number of field surveys carried out in 2013 in the Ningaloo Marine Park (see

Figure 16). We first describe a survey in the Maud Sanctuary Zone, on reef flat habitat which is typically shallow (<3 m) and dominated by tabulate coral of the genus *Acropora*. The survey was carried out before dusk with the use of 8 underwater cameras (Sony DCR-HC15E) in a housing mounted on a concrete block. Cameras recorded for around 3 hours. In the laboratory, video footage was then viewed on a computer screen and the amount of time spent by all sharks in the field of view was recorded. From these recordings, we calculated the observed frequency of shark detection, F_{obs} as described in Section 3. Like all measurements, estimates of F_{obs} are necessarily noisy. Recall that F_{obs} is a function of the time sharks are visible on the video. While current technology provides for a very accurate analysis of the visual recording (25 frames per second for our equipment), the visual field of a camera changes as a function of visibility, which depends on the time of the day, weather conditions, turbidity, currents etc. Since we do not have sufficient information to estimate the impact of these factors on a camera visual field, here we account for $\pm 10\%$ noise to the F_{obs} estimations. A careful analysis of the variation of visual field under different survey condition could improve on this estimate.

Figure 15 shows three F_{mod} plots for the Maud Sanctuary Zone field survey. Because this field survey was carried out at dusk, like [3] we assume the sharks were preferentially swimming towards the foraging area and thus we set $k_{dir} = 0.1$. Figure 15a shows the shark density estimates for all path types. Because of uncertainty on the value of the swimming speed, each path type was run with multiple swimming speeds (0.5, 0.7 and 1 m/s) and each swimming speed was considered equally likely. The confidence range in the plots in Figure 15a thus account for the uncertainty in swimming speeds. As expected, shark abundance assessment varies considerably, ranging from 11-31 (median ≈ 18) sharks/km² for JP1 to 13-111 (median ≈ 53) sharks/km² for BM.

Figure 15b shows the density estimates separately for each swimming speed (0.5, 0.7 and 1 m/s), where each swimming speed was run for all path types. Here too each path type was considered equally likely. Because the uncertainty on the path types has a much larger effect than the uncertainty on the swimming speed, in this panel the shark abundance assessments show less variability, ranging from 13-71 (median \approx 33) sharks/km² for swimming speed of 1 m/s, to 15-99 (median \approx 40) sharks/km² for swimming speed of 0.5 m/s. Finally, Figure 15c shows the overall uncertainty accounting for all path types and all swimming speeds, with a shark abundance assessments ranging from 14-85 (median \approx 37) sharks/km².

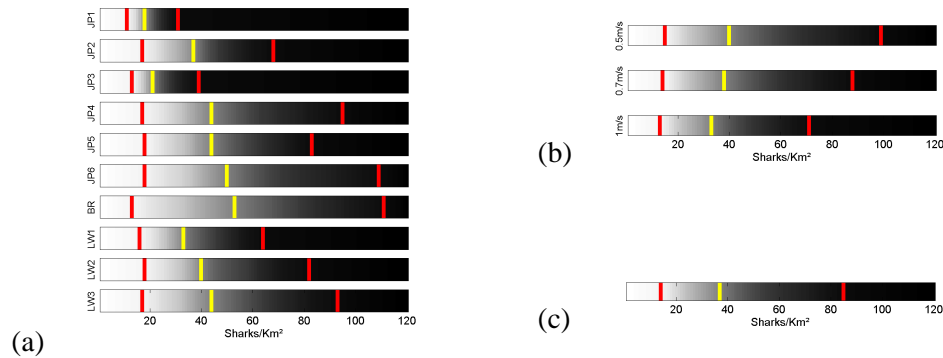


Figure 15. F_{mod} plots for field data collected at Maud Sanctuary Zone with $k_{dir}=0.1$, that is assuming sharks were foraging during the survey. (a) Shark density estimates for each of the path types, including the variation in swimming speed. (b) Shark density estimates for each of the three swimming speeds, incorporating varying path types. (c) Overall density estimations for varying swimming speeds and path types.

Finally,

Figure 16 Figure 16 shows the F_{mod} plots for seven different field surveys carried out in 2013 in the Ningaloo Marine Park. For each survey, Figure 16 shows the survey location within the Ningaloo Marine Park and the F_{mod} plots for path types JP1 (top survey panel) and BM (bottom) to provide extreme ranges in density estimation and its uncertainty. As in Figure 15a, each path type accounts for uncertainty in swimming speeds by including sharks swimming at 0.5, 0.7 and 1 m/s. The results show a wide range in estimates of density among the survey locations: the lowest estimates were recorded at Bundegi, and the highest (and most uncertain) estimates were recorded at Cloates. The confidence intervals for several locations did not overlap (e.g. Bundegi vs Osprey, giving high confidence that the different locations support different abundances of sharks).

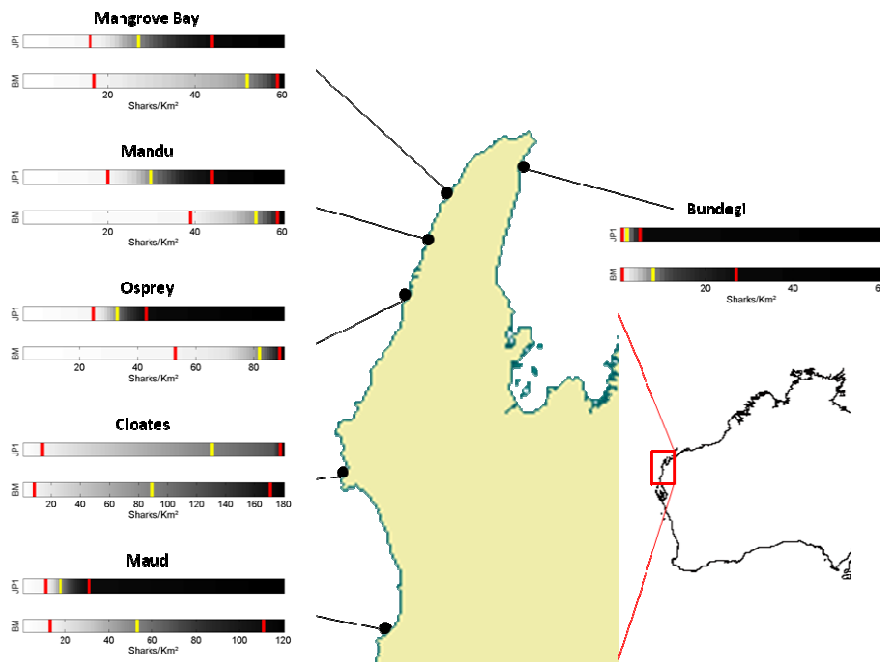


Figure 16. Abundance estimation for a number of field surveys carried out in 2013 in the Ningaloo Marine Park, Western Australia.

8 Discussion and conclusions

Assumptions about small scale movement characteristics of large predators can have a considerable impact on density estimates and the uncertainty associated with these estimates. This is true of movement characteristics which affect the population behaviour (like predator interactions) and of characteristics which only affect individual behaviour, like speed and site preference.

Our results show that, of characteristics of an individual's movement, three have by far the largest influence on estimates of abundance: i) average swimming speed; ii) whether or not individuals movement is oriented to particular locations (possibly dependent on the time of the day) and iii) the correlation length in the turning angles and step lengths which determines the larger scale statistical property of the swimming path. High correlation length (longer memory in directional changes, as in JP1) lead to lower density estimates and smaller uncertainty range; conversely, low (or zero) correlation length (shorter or no memory in directional changes, as in JP6 and BM) lead to higher density estimates and much larger uncertainty range. Lévy walk distributions lead to results similar to JP1 (lower density estimation and smaller uncertainty). Other factors affecting shark movement can impact on shark density assessment, but to a comparatively lesser extent.

As a result, an improved understanding of these three features of shark movement in natural environments can considerably improve our assessment of shark abundance and deserves further research effort. We believe that this effort should follow two directions. First, improvements in tracking devices and remote sensing technology can provide larger amount of data at higher temporal and spatial resolution. This is crucial given the paucity of information currently available on animal movement. In the context of this work, this type of information can greatly improve our understanding of habitat preference and foraging habits, thus leading to a better definition of the k_{dir} parameter, which has the largest impact on abundance estimates. It may also help better define the swimming speed, thus providing further improvement to the abundance estimates. However, as discussed in Section 2, the accurate assessment of the path types (JP1-6, BM, LW1-3) is difficult even with very good datasets, for a number of reasons which include the context dependence of swimming behaviour. As a result, we suggest that the second research direction should focus on more theoretical work. Our work suggests that the mean cosine angle (see Table 1) is related to abundance estimation, via its influence on the path correlation length and spatial extent

covered during the movement. Other large scale statistical properties of movement (return time, first passage time and diffusion coefficient) are worth investigating since they may be easier to measure in experimental settings and may provide indirect information about the path types. Given the magnitude of the impact these factors have on density estimates, even a relatively small improvements in their estimation may lead to considerable reduction in uncertainty. In our future work we will focus on both these research directions.

In this work we chose to emphasise the visual representation of our modelling results. This choice was driven by the belief that in the medium to long term, animal density estimates will necessarily continue to be largely uncertain and a visual appraisal of such uncertainty (and of how different parameters contribute to it), can help guide data analysis and further survey design as much as a purely numerical estimation of such an uncertainty, especially for users with little modelling expertise. This does not imply that further computational advances should not be pursued at the same time. In fact, computational and theoretical developments can not only provide better density assessments but also improve the very visual analysis we discussed above. From a theoretical point of view, this approach offers itself naturally to be extended via Bayesian Hierarchical Modelling [52-56] as explored in [57]. The promise is not only to make a formal use of a-priori ecological knowledge on shark behaviour, but also to provide probability distributions over the density assessments. From an implementation point of view, the approach requires a considerable computational effort which may force approximations or shortcuts in the model. We expect a combination of better instrumentations, further understanding of shark behaviour and computational advances will improve population density estimations and provide more accurate information for conservation decision making.

Acknowledgments

We thank Emy Guilbault, Monique Grol, Rosh McCallum, Damian Thomson, Mick Haywood, Auriane Jones and Russ Babcock for assistance in the field and laboratory.

References:

- [1] Pimm, S.L., Jenkins, C.N., Abell, R., Brooks, T.M., Gittleman, J.L., Joppa, L.N., Raven, P.H., Roberts, C.M. & Sexton, J.O. 2014 The biodiversity of species and their rates of extinction, distribution, and protection. *Science* **344**, 987-+. (doi:Artn 1246752
Doi 10.1126/Science.1246752).
- [2] Hughes, T.P., Bellwood, D.R., Connolly, S.R., Cornell, H.V. & Karlson, R.H. 2014 Double Jeopardy and Global Extinction Risk in Corals and Reef Fishes. *Curr Biol* **24**. (doi:DOI 10.1016/j.cub.2014.10.037).
- [3] Vanderklift, M., Boschetti, F., Roubertie, C., Pillans, R., Haywood, D. & Babcock, R. 2014 Using an agent-based model to estimate the density of reef sharks from video surveys. *Marine Ecology Progress Series* **In Print**.
- [4] McCauley, D.J., McLean, K.A., Bauer, J., Young, H.S. & Micheli, F. 2012 Evaluating the performance of methods for estimating the abundance of rapidly declining coastal shark populations. *Ecological Applications* **22**, 385-392. (doi:10.1890/11-1059.1).
- [5] Petrovskaya, N., Petrovskii, S. & Murchie, A.K. 2012 Challenges of ecological monitoring: estimating population abundance from sparse trap counts. *Journal of the Royal Society, Interface / the Royal Society* **9**, 420-435. (doi:10.1098/rsif.2011.0386).
- [6] Ward-Paige, C., Mills Flemming, J. & Lotze, H.K. 2010 Overestimating Fish Counts by Non-Instantaneous Visual Censuses: Consequences for Population and Community Descriptions. *PLoS ONE* **5**, e11722. (doi:10.1371/journal.pone.0011722).
- [7] Turnock, B.J. & Quinn II, T.J. 1991 The Effect of Responsive Movement on Abundance Estimation Using Line Transect Sampling. *Biometrics* **47**, 701-715.
- [8] Horne, J.S., Garton, E.O., Krone, S.M. & Lewis, J.S. 2007 Analyzing animal movements using Brownian bridges. *Ecology* **88**, 2354-2363. (doi:Doi 10.1890/06-0957.1).
- [9] Rees, S.G., Goodenough, A.E., Hart, A.G. & Stafford, R. 2011 Testing the effectiveness of capture mark recapture population estimation techniques using a computer simulation with known population size. *Ecological Modelling* **222**, 3291-3294. (doi:10.1016/j.ecolmodel.2011.05.030).
- [10] Chandler, R.B. & Royle, J.A. 2013 Spatially Explicit Models for Inference About Density in Unmarked or Partially Marked Populations. *Ann Appl Stat* **7**, 936-954. (doi:Doi 10.1214/12-Aoas610).
- [11] Zollner, P.A. & Lima, S.L. 1999 Search strategies for landscape-level interpatch movements. *Ecology* **80**, 1019-1030.

- [12] Rowcliffe, J.M., Field, J., Turvey, S.T. & Carbone, C. 2008 Estimating animal density using camera traps without the need for individual recognition. *J Appl Ecol* **45**, 1228-1236. (doi:DOI 10.1111/j.1365-2664.2008.01473.x).
- [13] Symons, J. & Boschetti, F. 2012 How Computational Models Predict the Behavior of Complex Systems. *Foundations of Science*, 1-13. (doi:10.1007/s10699-012-9307-6).
- [14] Tarantola, A. 1987 *Inverse Problem Theory*. Amsterdam, Elsevier.
- [15] Getz, W.M. & Saltz, D. 2008 A framework for generating and analyzing movement paths on ecological landscapes. *Proceedings of the National Academy of Sciences* **105**, 19066-19071. (doi:10.1073/pnas.0801732105).
- [16] Nathan, R., Getz, W.M., Revilla, E., Holyoak, M., Kadmon, R., Saltz, D. & Smouse, P.E. 2008 A movement ecology paradigm for unifying organismal movement research. *Proceedings of the National Academy of Sciences* **105**, 19052-19059. (doi:10.1073/pnas.0800375105).
- [17] Fronhofer, E.A., Hovestadt, T. & Poethke, H.-J. 2012 From random walks to informed movement. *Oikos*, no-no. (doi:10.1111/j.1600-0706.2012.21021.x).
- [18] Crist, T.O., Guertin, D.S., Wiens, J.A. & Milne, B.T. 1992 Animal Movement in Heterogeneous Landscapes - an Experiment with Eleodes Beetles in Shortgrass Prairie. *Funct Ecol* **6**, 536-544. (doi:Doi 10.2307/2390050).
- [19] Barraquand, F. & Benhamou, S. 2008 Animal Movements in Heterogeneous Landscapes: Identifying Profitable Places and Homogeneous Movement Bouts. *Ecology* **89**, 3336-3348. (doi:Doi 10.1890/08-0162.1).
- [20] Benhamou, S. 2014 Of scales and stationarity in animal movements. *Ecology Letters* **17**, 261-272. (doi:Doi 10.1111/Ele.12225).
- [21] James, A., Plank, M.J. & Edwards, A.M. 2011 Assessing Lévy walks as models of animal foraging. *Journal of the Royal Society, Interface / the Royal Society* **8**, 1233-1247. (doi:10.1098/rsif.2011.0200).
- [22] Reynolds, A.M., Smith, A.D., Menzel, R., Greggers, U., Reynolds, D.R. & Riley, J.R. 2007 Displaced honey bees perform optimal scale-free search flights. *Ecology* **88**, 1955-1961.
- [23] Reynolds, a.M. 2012 Fitness-maximizing foragers can use information about patch quality to decide how to search for and within patches: optimal Levy walk searching patterns from optimal foraging theory. *Journal of the Royal Society, Interface / the Royal Society* **9**, 1568-1575. (doi:10.1098/rsif.2011.0815).
- [24] Humphries, N.E., Weimerskirch, H., Queiroz, N., Southall, E.J. & Sims, D.W. 2012 Foraging success of biological Levy flights recorded in situ. *P Natl Acad Sci USA*, 1-6. (doi:10.1073/pnas.1121201109).
- [25] Sims, D.W., Humphries, N.E., Bradford, R.W. & Bruce, B.D. 2012 Lévy flight and Brownian search patterns of a free-ranging predator reflect different prey field characteristics. *The Journal of animal ecology* **81**, 432-442. (doi:10.1111/j.1365-2656.2011.01914.x).
- [26] Palyulin, V.V., Chechkin, A.V. & Metzler, R. 2014 Lévy flights do not always optimize random blind search for sparse targets. *Proceedings of the National Academy of Sciences* **111**, 2931-2936. (doi:10.1073/pnas.1320424111).
- [27] Bartumeus, F., Catalan, J., Fulco, U., Lyra, M. & Viswanathan, G. 2002 Optimizing the Encounter Rate in Biological Interactions: Lévy versus Brownian Strategies. *Physical Review Letters* **88**, 2-5. (doi:10.1103/PhysRevLett.88.097901).
- [28] Viswanathan, G.M., Buldyrev, S.V., Havlin, S., da Luz, M.G., Raposo, E.P. & Stanley, H.E. 1999 Optimizing the success of random searches. *Nature* **401**, 911-914. (doi:10.1038/44831).
- [29] Kawai, R. & Petrovskii, S. 2012 Multi-scale properties of random walk models of animal movement: lessons from statistical inference. *Proceedings of the Royal Society A: Mathematical, Physical and Engineering Science* **468**, 1428-1451. (doi:10.1098/rspa.2011.0665).
- [30] Bartumeus, F., Catalan, J., Viswanathan, G.M., Raposo, E.P. & da Luz, M.G.E. 2008 The influence of turning angles on the success of non-oriented animal searches. *J Theor Biol* **252**, 43-55. (doi:10.1016/j.jtbi.2008.01.009).
- [31] Kareiva, P.M. & Shigesada, N. 1983 Analyzing insect movement as a correlated random walk. *Oecologia* **56**, 234-238. (doi:10.1007/BF00379695).
- [32] Gautestad, A.O. 2012 Animal space use: distinguishing a two-level superposition of scale-specific walks from scale-free Lévy walk. *Oikos*, no-no. (doi:10.1111/j.1600-0706.2012.19998.x).
- [33] Bartumeus, F. 2009 Behavioral intermittence, LEvy patterns, and randomness in animal movement. *Oikos* **118**, 488-494. (doi:DOI 10.1111/j.1600-0706.2009.17313.x).
- [34] Jansen, V.A.A., Mashanova, A. & Petrovskii, S. 2012 Comment on "Levy Walks Evolve Through Interaction Between Movement and Environmental Complexity". *Science* **335**. (doi:DOI 10.1126/science.1215747).
- [35] Reynolds, A.M. 2012 Distinguishing between Levy walks and strong alternative models. *Ecology* **93**, 1228-1233.
- [36] Bartumeus, F., da Luz, M.G.E., Viswanathan, G.M. & Catalan, J. 2005 Animal search strategies: a quantitative random walk analysis. *Ecology* **86**, 3078-3087.
- [37] Sakiyama, T. & Gunji, Y.P. 2013 Emergence of an optimal search strategy from a simple random walk. *J R Soc Interface* **10**. (doi:Artn 20130486
Doi 10.1098/Rsif.2013.0486).

- [38] Edwards, A.M., Phillips, R.a., Watkins, N.W., Freeman, M.P., Murphy, E.J., Afanasyev, V., Buldyrev, S.V., da Luz, M.G.E., Raposo, E.P., Stanley, H.E., et al. 2007 Revisiting Lévy flight search patterns of wandering albatrosses, bumblebees and deer. *Nature* **449**, 1044-1048. (doi:10.1038/nature06199).
- [39] Sims, D.W., Righton, D. & Pitchford, J.W. 2007 Minimizing errors in identifying Lévy flight behaviour of organisms. *The Journal of animal ecology* **76**, 222-229. (doi:10.1111/j.1365-2656.2006.01208.x).
- [40] Zollner, P.A. & Lima, S.L. 1999 Search strategies for landscape-level interpatch movements. *Ecology* **80**, 1019-1030. (doi:Doi 10.1890/0012-9658(1999)080[1019:Ssflil]2.0.Co;2).
- [41] Codling, E.A. & Hill, N.A. 2005 Sampling rate effects on measurements of correlated and biased random walks. *J Theor Biol* **233**, 573-588. (doi:DOI 10.1016/j.jtbi.2004.11.008).
- [42] Patrick, S.C., Bearhop, S., Gremillet, D., Lescroel, A., Grecian, W.J., Bodey, T.W., Hamer, K.C., Wakefield, E., Le Nuz, M. & Votier, S.C. 2014 Individual differences in searching behaviour and spatial foraging consistency in a central place marine predator. *Oikos* **123**, 33-40. (doi:DOI 10.1111/j.1600-0706.2013.00406.x).
- [43] Ferreira, A.S., Raposo, E.P., Viswanathan, G.M. & da Luz, M.G.E. 2012 The influence of the environment on Lévy random search efficiency: Fractality and memory effects. *Physica A: Statistical Mechanics and its Applications* **391**, 3234-3246. (doi:10.1016/j.physa.2012.01.028).
- [44] Benhamou, S. 2012 How Many Animals Really Do the Lévy Walk ? *Ecology* **88**, 1962-1969.
- [45] Humphries, N.E., Queiroz, N., Dyer, J.R.M., Pade, N.G., Musyl, M.K., Schaefer, K.M., Fuller, D.W., Brunnschweiler, J.M., Doyle, T.K., Houghton, J.D.R., et al. 2010 Environmental context explains Lévy and Brownian movement patterns of marine predators. *Nature* **465**, 1066-1069. (doi:10.1038/nature09116).
- [46] Parker, R. 1977 Understanding inverse theory. *Annual Review of Earth and Planetary Sciences* **5**, 35-64.
- [47] Boschetti, F. 2008 Mapping the complexity of ecological models. *Ecological Complexity* **5**, 37-47.
- [48] Boschetti, F. 2010 Detecting behaviours in ecological models. *Ecological Complexity* **7**, 76-85. (doi:10.1016/j.ecocom.2009.05.014).
- [49] Boschetti, F., Wijns, C. & Moresi, L. 2003 Effective exploration and visualization of geological parameter space. *Geochemistry Geophysics Geosystems* **4**. (doi:1086 10.1029/2002gc000503).
- [50] Stuart, A.M. 2010 Inverse problems: A Bayesian perspective. *Acta Numerica* **19**, 451-559. (doi:doi:10.1017/S0962492910000061).
- [51] Dowd, M. & Meyer, R. 2003 A Bayesian approach to the ecosystem inverse problem. *Ecological Modelling* **168**, 39-55. (doi:Doi 10.1016/S0304-3800(03)00186-8).
- [52] Schick, R.S., Loarie, S.R., Colchero, F., Best, B.D., Boustany, A., Conde, D.A., Halpin, P.N., Joppa, L.N., McClellan, C.M. & Clark, J.S. 2008 Understanding movement data and movement processes: current and emerging directions. *Ecology Letters* **11**, 1338-1350. (doi:DOI 10.1111/j.1461-0248.2008.01249.x).
- [53] Andrieu, C., Doucet, A. & Holenstein, R. 2010 Particle Markov chain Monte Carlo methods. *J R Stat Soc B* **72**, 269-342.
- [54] Doucet, A., Godsill, S. & Andrieu, C. 2000 On sequential Monte Carlo sampling methods for Bayesian filtering. *Stat Comput* **10**, 197-208. (doi:Doi 10.1023/A:1008935410038).
- [55] Parslow, J., Cressie, N., Campbell, E.P., Jones, E. & Murray, L. 2013 Bayesian learning and predictability in a stochastic nonlinear dynamical model. *Ecological Applications* **23**, 679-698.
- [56] Jones, E., Parslow, J. & Murray, L. 2010 A Bayesian approach to state and parameter estimation in a Phytoplankton-Zooplankton model. *Aust Meteorol Ocean* **59**, 7-15.
- [57] Breed, G.a., Costa, D.P., Jonsen, I.D., Robinson, P.W. & Mills-Flemming, J. 2012 State-space methods for more completely capturing behavioral dynamics from animal tracks. *Ecological Modelling* **235-236**, 49-58. (doi:10.1016/j.ecolmodel.2012.03.021).
- [58] Mantegna, R.N. 1994 Fast, accurate algorithm for numerical simulation of Levy stable stochastic processes. *Physical Review E* **49**, 4677-4688.
- [59] Edwards, A.M. 2008 Using likelihood to test for Lévy flight search patterns and for general power-law distributions in nature. *The Journal of animal ecology* **77**, 1212-1222. (doi:10.1111/j.1365-2656.2008.01428.x).
- [60] Clauset, A., Shalizi, C.R. & Newman, M.E.J. 2009 Power-Law Distributions in Empirical Data. *Siam Rev* **51**, 661-703. (doi:Doi 10.1137/070710111).
- [61] Jones, M.C. & Pewsey, A. 2005 A family of symmetric distributions on the circle. *Journal of the American Statistical Association* **100**, 1422-1428. (doi:Doi 10.1198/016214505000000286).
- [62] Abe, T., Shimizu, K. & Pewsey, A. 2010 Symmetric unimodal models for directional data motivated by inverse stereographic projection. *Journal of the Japan Statistical Society*. **40**, 45-61.
- [63] Codling, E.A., Hill, N.A., Pitchford, J.W. & Simpson, S.D. 2004 Random walk models for the movement and recruitment of reef fish larvae. *Marine Ecology Progress Series* **279**, 215-224. (doi:Doi 10.3354/Meps279215).
- [64] Sims, D.W., Southall, E.J., Humphries, N.E., Hays, G.C., Bradshaw, C.J., Pitchford, J.W., James, A., Ahmed, M.Z., Brierley, A.S., Hindell, M.a., et al. 2008 Scaling laws of marine predator search behaviour. *Nature* **451**, 1098-1102. (doi:10.1038/nature06518).

- [65] Viswanathan, G.M., Afanasyev, V., Buldyrev, S.V., Murphy, E.J., Prince, P.A. & Stanley, H.E. 1996 Levy flight search patterns of wandering albatrosses. *Nature* **381**, 413-415.
- [66] Marell, A., Ball, J.P. & Hofgaard, A. 2002 Foraging and movement paths of female reindeer: insights from fractal analysis, correlated random walks, and Levy flights. *Canadian Journal of Zoology* **80**, 854-865. (doi:Doi 10.1139/Z02-061).
- [67] Reynolds, A.M., Smith, A.D., Menzel, R., Greggers, U., Reynolds, D.R. & Riley, J.R. 2007 Displaced honey bees perform optimal scale-free search flights. *Ecology* **88**, 1955-1961.
- [68] Reynolds, A.M., Smith, A.D., Reynolds, D.R., Carreck, N.L. & Osborne, J.L. 2007 Honeybees perform optimal scale-free searching flights when attempting to locate a food source. *Journal of Experimental Biology* **210**, 3763-3770. (doi:Doi 10.1242/Jeb.009563).
- [69] Sims, D.W., Humphries, N.E., Bradford, R.W. & Bruce, B.D. 2012 Lévy flight and Brownian search patterns of a free-ranging predator reflect different prey field characteristics. *Journal of Animal Ecology* **81**, 432-442. (doi:10.1111/j.1365-2656.2011.01914.x).
- [70] James, A., Plank, M.J. & Edwards, A.M. 2011 Assessing Lévy walks as models of animal foraging. *Journal of the Royal Society Interface* **8**, 1233-1247. (doi:10.1098/rsif.2011.0200).
- [71] Reynolds, A.M. 2012 Truncated Lévy walks are expected beyond the scale of data collection when correlated random walks embody observed movement patterns. *Journal of the Royal Society Interface* **9**, 528-534. (doi:10.1098/rsif.2011.0363).
- [72] Viswanathan, G.M., Raposo, E.P. & da Luz, M.G.E. 2008 Lévy flights and superdiffusion in the context of biological encounter and random searches. *ScienceDirect* **5**, 133-150.
- [73] Press, W.H. 1996 *Numerical recipes in fortran 77 : the art of scientific computing*. 2nd ed. Cambridge England ; New York, Cambridge University Press; xxxi, 933 p. p.
- [74] Hornby, P., Boschetti, F. & Horowitz, F.G. 1999 Analysis of potential field data in the wavelet domain. *Geophysical Journal International* **137**, 175-196. (doi:DOI 10.1046/j.1365-246x.1999.00788.x).
- [75] Blakely, R.J. 1995 *Potential theory in gravity and magnetic applications*. Cambridge England ; New York, Cambridge University Press; xix, 441 p. p.
- [76] Nams, V.O. 2006 Detecting oriented movement of animals. *Animal Behaviour* **72**, 1197-1203. (doi:10.1016/j.anbehav.2006.04.005).
- [77] McCauley, D.J., McLean, K.A., Bauer, J., Young, H.S. & Micheli, F. 2012 Evaluating the performance of methods for estimating the abundance of rapidly declining coastal shark populations. *Ecological Applications* **22**, 385-392.
- [78] Sundström, L.F., Gruber, S.H., Clermont, S.M., Correia, J.P.S., de Marignace, J.R.C., Morrissey, J.F., Lowrance, C.R., Thomassen, L. & Oliveira, M.T. 2001 Review of elasmobranch behavioral studies using ultrasonic telemetry with special reference to the lemon shark, *Negaprion brevirostris*, around Bimini Islands, Bahamas. *Environmental Biology of Fishes* **60**, 225-250.
- [79] Webb, P.W. & Keyes, R.S. 1982 Swimming kinematics of sharks. *Fishery Bulletin* **80**, 803-812.

How the movement characteristics of large marine predators affect estimates of their abundance

Supplementary Material

1. Appendix – Model flowchart

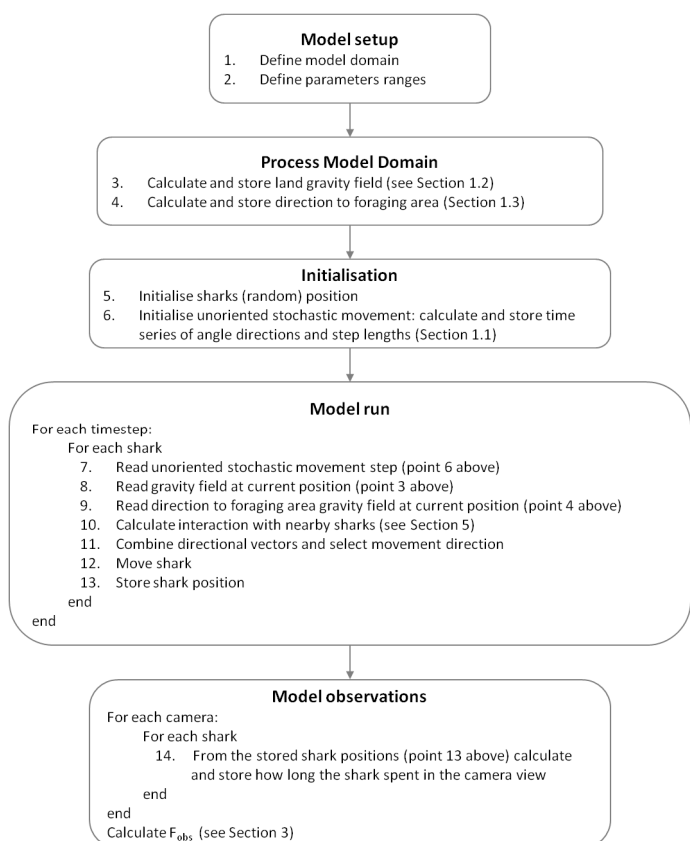
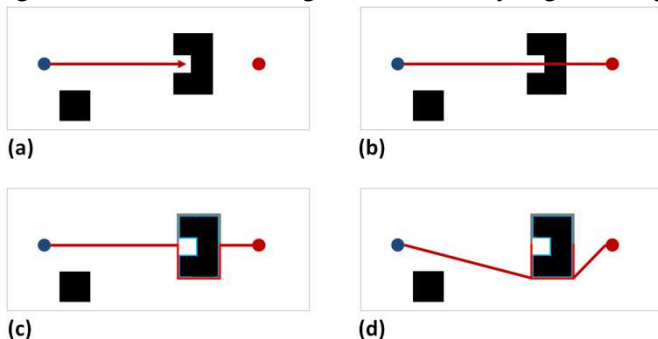


Figure 1. Model Flowchart.

2. Appendix – the path-finding algorithm

The aim of this module is to guide the predator to a target location while avoiding local physical obstacles like reefs and coastlines. Different types of algorithms are available in the literature to address similar problems, including ray-tracing algorithms used in computer vision to model light diffusion, reflections and refractions, ray-tracing algorithms used in seismic modelling to model underground acoustic wave propagation and motion tracking algorithms used in robotics to control the movement of autonomous agents. The algorithm we describe here belongs to the latter class.

In general, most of these algorithms work by i) generating feasible paths from the source, ii) following the paths



until the target is reached and iii) if more than one path reaches the target, choosing the one which is optimal according to specific criteria (distance covered, travel-time, cost, etc). In principle we could implement this scheme via a gravity field, as we did to avoid the coastline in Section **Error! Reference source not found.** and described in Appendix 3, by i) placing the source of a gravitation field at the target location, ii) assigning a gravitational field of opposite sign to obstacles and iii) letting the predator navigate this gravity field. However, this way a predator could get trapped in a gravity local minima, as shown in Figure 2a, thus being unable to reach the target. This could be circumvented only by allowing the predator to explore alternative paths, with considerable increase in computational effort.

Figure 2. Schematic description of the obstacle avoidance algorithm. The blue dot is the predator starting location, the red dot the target and an obstacle is placed along the way.

Here we implement an alternative approach which consists in i) first drawing a direct path to the target (this path may not be viable since it may cross an obstacle) and then ii) modify the path until it becomes viable. The algorithm can be summarised as follows:

- 1) Draw a straight line from the starting point to the target as in Figure 2b; call this *current path*;
- 2) For each obstacle, generate its *convex hull* and store it as the effective border of the obstacle.
- 3) If an intersection exists between the *current path* and an obstacle, we first check whether it is faster to circumnavigate the obstacle along the *convex hull* clockwise or counter-clockwise; we call this *detour*. Then, we remove from the *current path* the section within the convex hull and replace it with the *detour*, as in Figure 2c. This represents the new *current path*.
- 4) Finally, if the *current path* is viable along its full extent we straighten unnecessary irregularities, as in Figure 2d.
- 5) The *current path* may now cross a new obstacle, in which case we go to point 2.

The algorithm does not guarantee that an optimal path is found. For the purpose of this work, optimality is not specifically required (we do not know if predators follow optimal paths) but we want to ensure that the target is reached at the end of the path. In Figure 3 we show some particularly challenging applications of the algorithm, for demonstrational purposes.

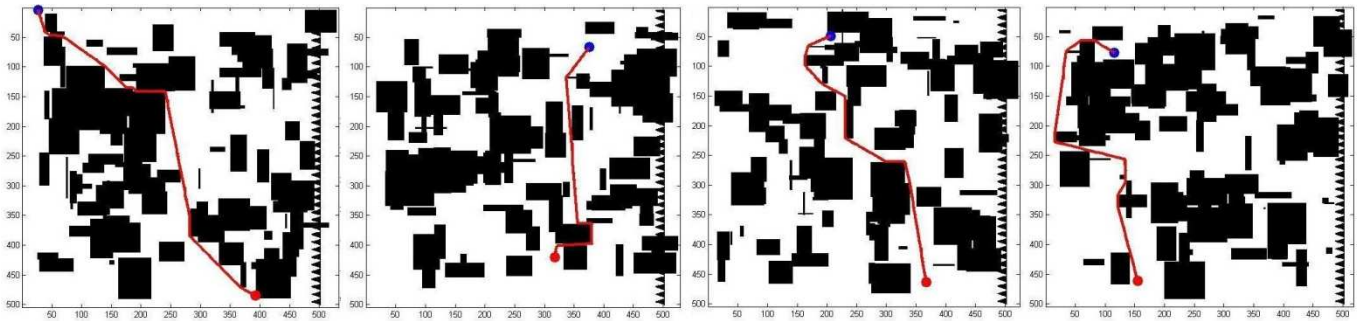


Figure 3. Examples of swimming paths in very complex environment, for demonstrational purposes. Sharks start from the blue dot and aim to reach the target at the red dot.

3. Appendix – Gravity field use in obstacle avoidance and shark interaction

Given the gravitational potential V at point (x,y,z) due to a body of mass ρ (Source), where G is the gravitational constant [1]

$$V(x, y, z) = -G \int_{Source} \frac{\rho dx' dy' dz'}{((x - x')^2 + (y - y')^2 + (z - z')^2)^{1/2}}$$

Equation 1

the horizontal gravitational attraction over the X axis (and similarly over the Y and Z axis) is given by

$$\frac{\partial \mathcal{V}}{\partial x} = G \int_{Source} \frac{\rho(x-x')dx'dy'dz'}{((x-x')^2 + (y-y')^2 + (z-z')^2)^{3/2}}$$

Equation 2

The strength of the gravitational attraction thus depends on i) the mass of the source (ρ), ii) its shape over (x',y',z') and iii) the distance from the source.

Our model is two dimensional since we do not account for depth, so in principle we have $z=z'$. This can generate singularities in the computation of the gravity attraction [2]. We thus calculate the gravity attraction at a fictitious height $z=z_0$ from the source as in Equation 3.

$$\frac{\partial \mathcal{V}}{\partial x} = G \int_{Source} \frac{\rho(x-x')dx'dy'dz'}{((x-x')^2 + (y-y')^2 + (z_0-z')^2)^{3/2}}$$

Equation 3

Naturally, the larger z_0 , the smoother the field $\frac{\partial \mathcal{V}}{\partial x}$ (same over the Y axis) [3].

In our model the gravitational attraction is used both to allow a shark to avoid physical obstacles (repulsion from land and reef crests) and to interact with other sharks (attraction or repulsion). As a result, the source of the gravitational field can be the land and reef crests as well as near-by sharks. Equation 3 allows us to control the shape of the gravitational attraction via two parameters: i) ρ (mass of the land, reef or near-by shark) controls the strength of the attraction as well as its sign (attraction or repulsion) and ii) z_0 controls how fast the attraction diminishes with (horizontal) distance from the source, effectively determining the range over which gravitational attraction acts on the shark.

References:

1. Blakely, R.J., *Potential theory in gravity and magnetic applications*. 1995, Cambridge England ; New York: Cambridge University Press. xix, 441 p.
2. Trompat, H., F. Boschetti, and P. Hornby, *Improved downward continuation of potential field data*. Exploration Geophysics, 2003. **34**(4): p. 249-256.
3. Hornby, P., F. Boschetti, and F.G. Horowitz, *Analysis of potential field data in the wavelet domain*. Geophysical Journal International, 1999. **137**(1): p. 175-196.